HYDROGEN DIFFUSION IN THE VICINITY OF A CRACK TIP AFTER CYCLIC PRE-LOADING

V. Kharin and J. Toribio
Department of Materials Engineering, University of Salamanca
E.P.S., Campus Viriato, Avda. Requejo 33, 49022 Zamora
Tel: 980 545 000; Fax: 980 545 002, E-mail: toribio@usal.es

Abstract. In this paper, a numerical analysis is performed of the effect of cyclic pre-loading regime on the posterior hydrogen assisted cracking behaviour of high-strength steel, considering mechanical items (stress-strain evolution) and chemical aspects (hydrogen diffusion). With regard to mechanical issues, a high resolution numerical modelling is carried out of the elastoplastic stress-strain field in the near-tip area under cyclic loading (to simulate fatigue pre-cracking) and posterior monotonic loading (to simulate a slow strain rate test), considering the role of large near-tip deformations. In the matter of chemical aspects, a quantitative modelling of hydrogen diffusion is performed near the crack tip, accounting for the transient stress-strain field that evolves from the compressive one after pre-cracking to the tensile one during the test. Results show that hydrogen accumulation in fracture sites depends on residual stress distributions produced by cyclic pre-loading.

Resumen. En este artículo se lleva a cabo un análisis numérico del efecto del régimen de pre-carga cíclica sobre el comportamiento posterior de acero de alta resistencia en condiciones de fisuración asistida por hidrógeno, considerando tanto aspectos mecánicos (evolución tenso-deformacional) como químicos (difusión de hidrógeno). Con respecto a cuestiones mecánicas, se realiza una modelización numérica de alta resolución del campo tenso-deformacional elastoplástico en el área próxima a la fisura bajo carga cíclica (para simular la pre-fisuración por fatiga) y carga posterior monótona creciente (para simular el ensayo a velocidad de deformación lenta), considerando el papel de las grandes deformaciones junto al extremo de la fisura. En lo que se refiere a los aspectos químicos, se modeliza de forma cuantitativa la difusión de hidrógeno cerca de la fisura, teniendo en cuenta el carácter transitorio del campo tenso-deformacional que evoluciona de compresiones a tracciones durante el ensayo. Los resultados muestran que la acumulación de hidrógeno en los lugares de fractura depende del campo de tensiones residuales producido mediante la pre-carga cíclica.

1. INTRODUCTION

In the framework of fracture mechanics, experimental evaluation of environmentally assisted cracking (EAC) of materials is commonly performed in a laboratory by testing pre-cracked specimens. In this procedure, a pre-crack in the sample is required for posterior EAC testing, and it is usually generated by fatigue (cyclic) loading in air environment.

The procedure of fatigue precracking inevitably produces ambiguous mechanical effects in the near-tip area (cf. [*1*]), since the cyclic loading regime affects the plastic zone development and controls the evolution of stress-strain fields in the close vicinity of the crack tip after loading and unloading of the samples.

This paper analyzes a wide range of experimental results of slow strain rate (SSR) tests on high-strength steel in aqueous environments under cathodic electrochemical conditions promoting the phenomenon of *hydrogen assisted cracking* (HAC). Emphasis is placed on the effect of the previous fatigue pre-cracking procedure, which influences dramatically the behaviour of the steel in the posterior SSR test in a hydrogen environment.

2. EXPERIMENTAL

The aim is to analyze the consequences of fatigue pre-cracking on the posterior stress corrosion behaviour of the high-strength steel. Different zero-to-tension cyclic loading levels were used in the experiments, the key variable being the maximum stress intensity factor at the last stage of the pre-cracking K_{max}, whereas $K_{min} \approx 0$ in all tests. Four different fatigue programs were performed with K_{max}/K_{IC}= 0.28, 0.45, 0.60 and 0.80, where K_{IC} is the standard fracture toughness of the steel.

A high-strength steel was studied with eutectoid chemical composition and the following mechanical properties: Young modulus E= 195 GPa, yield strength σ_Y= 725 MPa, UTS σ_R = 1300 MPa, fracture toughness K_{IC} = 53 MPam$^{1/2}$. The EAC experiments were SSR tests with pre-cracked specimens in aqueous solution, as described in detail elsewhere [*2*]. The tests analyzed in this paper were performed at cathodic potentials to evaluate the HAC phenomenon as a key mechanism of

EAC. Fig. 1 shows the experimental results of the failure load in solution F_{HAC} (divided by the reference value at rupture in air F_C) as a function of the ratio K_{max}/K_{IC}. The mechanical effect of fatigue pre-cracking is beneficial for the HAC resistance of the steel, since the fracture load in hydrogen is an increasing function of K_{max}. In the matter of microscopic fracture modes, a special topography associated with hydrogen effects was found: the *tearing topography surface* (TTS) [*3*], so that the size of the TTS region is an indicator of the extension of hydrogen assisted micro-damage. In Fig. 2 a plot is given of the TTS depth vs. K_{max}. The higher the fatigue pre-cracking load, the lower the extension of the TTS domain (lower effect of hydrogen).

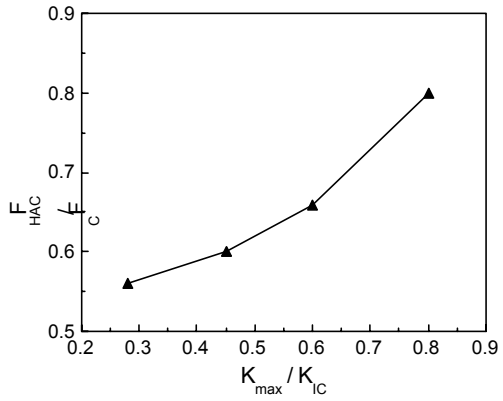

Fig. 1. SSR test results in terms of respective fracture loads in aggressive (hydrogen) and inert (laboratory air) environments as a function of K_{max} (average values [2]).

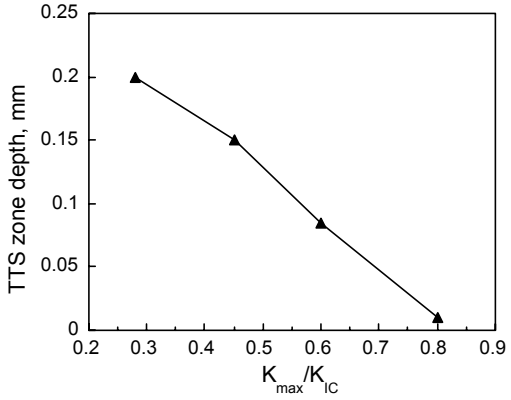

Fig. 2. TTS depth as a function of K_{max}.

These phenomena may be caused by the development of the cyclic plastic zone and the presence of compressive stresses (cyclic residual stresses) in the vicinity of the crack tip as a consequence of the fatigue pre-cracking procedure. The crack tip is pre-strained (and in a certain sense pre-stressed) by fatigue: the higher the cyclic load level, the more pronounced is the pre-straining/stressing effect, which delays the hydrogen entry into the metal and improves material performance.

To ascertain the mechanical effects of the pre-cracking regime on EAC, it is desired to know the evolution of certain mechanical variables associated with the environmentally assisted cracking processes. The item of primary interest is the stress distribution beyond the crack tip affected by cyclic pre-loading. In particular, hydrostatic stress σ plays a fundamental role in HAC driven by stress assisted hydrogen diffusion [*4*].

3. MECHANICAL MODELLING: TIME EVOLUTION OF STRESS-STRAIN FIELDS IN THE VICINITY OF THE CRACK TIP

The effect of fatigue pre-cracking is analyzed by high-resolution numerical modelling of the stress-strain state near the crack tip in a rate-independent elastoplastic material with von Mises yield surface and power-law strain hardening (isotropic-to-kinematic hardening rule is used [*5*]). The mechanical properties of the material correspond to the steel used in the experiments. Stress-strain fields in the close vicinity of the crack tip are known to depend substantially on the crack blunting [*6,7*]. To reveal them, finite deformation analysis of a plane strain crack subjected to mode I (opening) load was performed, confining the study to the small scale yielding situation, which allows a consideration of the stress intensity factor K as the only variable governing the near tip mechanical situation irrespective of a particular geometry of a cracked solid and applied load (cf. [*6,8*]). The crack was modelled as a parallel-sided round-tip slit with initial height (twice the tip radius) b_0 = 5 μm, which is in agreement with experimental data reported for fatigue cracks in steels [*9*]. The applied loading history consisted of several (up to ten) zero-to-tension cycles at K_{max}/K_{IC}= 0.45 and 0.80, followed by rising load corresponding to the SSR testing. The nonlinear finite element code MARC [*10*] was used with updated Lagrangian formulation. The modelling peculiarities are the same as described elsewhere [*7*]. The finite element mesh near the crack tip had four-node quadrilateral elements of the average size $0.02b_0$.

Fig. 3 shows the evolution of the hydrostatic stress distribution in the plane of the crack beyond the tip $\sigma(x)$, during monotonic loading in the SSR tests after fatigue pre-cracking, where x is the distance from the crack tip in the *deformed configuration* of the solid and thus x=0 represents the crack tip itself, i.e., the surface of the solid which determines the boundary condition for the problem of hydrogen diffusion in the solid. This figure provides a first insight (based on purely mechanical considerations) into the consequences of fatigue pre-stressing on the posterior HAC behaviour of the steel. For an intermediate level of externally applied loading in the SSR test (applied K= 0.30 K_{IC}), clear differences may be observed between the two distributions of hydrostatic stress (those associated with fatigue pre-cracking levels of K_{max} = 0.45 and 0.80 K_{IC}), especially in the close vicinity of the crack tip, which implies a different rate of hydrogen transport to prospective fracture nuclei by stress assisted diffusion according to which hydrogen is driven by the gradient of hydrostatic stress $d\sigma/dx$ [*4*].

In the case of the strongest fatigue program (K_{max} = 0.80 K_{IC}) it is seen in Fig. 3b that residual stresses

remain compressive in an extended area beyond the crack tip and, what is more important, there is a negative gradient of hydrostatic stress $d\sigma/dx<0$ that delays hydrogen diffusion to the inner points, prevents hydrogen degradation of the material therein, and increases the fracture load in a hydrogen environment.

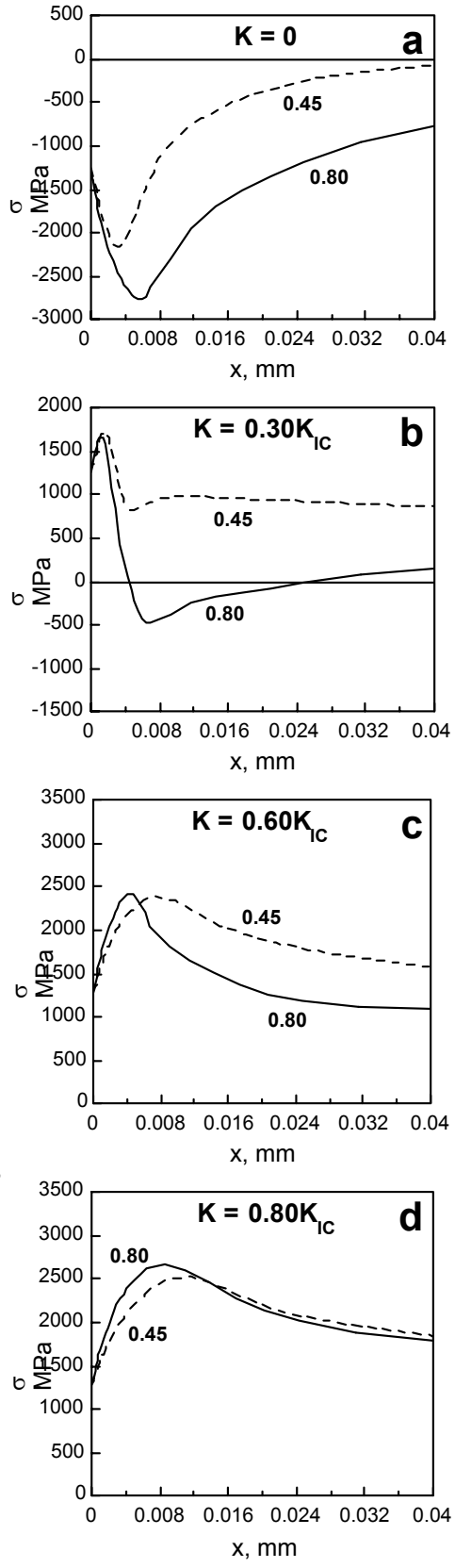

Fig. 3. Hydrostatic stress distributions ahead of the crack tip during monotonic loading at SSR test after fatigue pre-cracking at K_{max}/K_{IC} = 0.45 (dashed lines) and 0.80 (solid lines) at progressive applied K levels indicated in the figures. The distance x from the crack tip is measured in the deformed configuration.

Another assumption of increasing trapping of hydrogen after heavier fatigue pre-cracking is also consistent with the observed beneficial effect of K_{max} on posterior HAC resistance (Fig. 1): accumulated mechanical pre-damage in the cyclic plastic zone delays the hydrogen delivery due to an increase of the dislocation density and therefore of the number of potential hydrogen traps [*11*]. The higher the K_{max}, the larger the region of high traps density and the lower the hydrogen permeation rate.

4. MODELLING OF HYDROGEN DIFFUSION: EVOLUTION OF NEAR-TIP CONCENTRATION

4.1. Diffusional theory of HAC

Hydrogen effect on fracture depends on its amount in prospective rupture sites represented by the value of its volume concentration C which is provided there by hydrogen diffusion from external (environmental) or internal (residual hydrogen) sources. Local rupture occurs when in a relevant material element (cell, or "grain", or whichever point of interest) the concentration achieves the critical value C_{cr} determined, in general [*12,13*], by the principal components of stresses and (plastic) strains, respectively, σ_i and ε_i (i = 1,2,3)

$$C_{cr} = C_{cr}\,(\sigma_i,\, \varepsilon_i) \qquad (1)$$

The crack situated along the x-axis grows when hydrogen concentration accumulated with time t in a point $x = x_c$ attains the critical level corresponding to the instantaneous stress intensity factor $K(t)$

$$C(x_c,t) = C_{cr}\,(K(t),\, x_c) \qquad (2)$$

where the value of x_c must be defined with the concept of the responsible material cell, i.e., the worst material unit, weak grain, microstructural length, etc. [*4, 12-16*].

Local rupture repeatedly occurs whilst concentration of accumulated hydrogen $C(x,t)$ can satisfy the criterion (2) after finite diffusion times Δt. Then the crack advances by its size increments Δa which render macroscopic crack growth rate $v = \Delta a/\Delta t$. Impossibility to fulfil the criterion (2) with a certain K value at finite time means crack arrest (v = 0). This is associated with the steady-state (obviously, equilibrium) hydrogen concentration distribution in metal $C_\infty(K,x)$ attained at $t \to \infty$. C_∞ defines the extreme hydrogenation at a given stress intensity factor. Then, using this steady-state solution $C_\infty(K,x)$ in the criterion (2), this latter yields the equation to find the upper limit of K with which crack

growth rate $v = 0$. Thus, C_∞ determines the threshold stress intensity factor value K_{IHAC} for HAC.

The driving force X_D for diffusion is derived as [*12,17*]

$$X_D = -\nabla \text{ ¡Error!} \qquad (3)$$

where R is the universal gas constant, T the absolute temperature and K_S the solubility. The coefficient of diffusion of hydrogen in metal D defines its mobility equal to D/RT, which together with the driving force (3) yield the diffusion flux **J** of hydrogen in metal

$$\mathbf{J} = \text{¡Error!} C\, X_D \qquad (4)$$

The solubility K_S and the diffusivity D are known to depend on alloy and on density of hydrogen traps in the lattice [*11*]. Trap density and, in certain alloys, their phase composition, e.g., like martensite formation in austenitic steels [*18,19*], both depend on plastic deformation, which may be incorporated in terms of the effective plastic strain ε_p [*20*]. In addition, K_S depends on the hydrostatic stress σ and is given by [*12,20*]

$$K_S(\sigma, \varepsilon_p, T) = K_{S\varepsilon}(\varepsilon_p, T) \exp(\Omega\sigma)$$
$$\text{with } \Omega = \text{¡Error!} \qquad (5)$$

where $K_{S\varepsilon}$ is the strain-only dependent component of solubility and V_H the partial molar volume of hydrogen in metal. According to eqs. (3)-(5), the gradients of both ε_p and σ are governing factors of diffusion.

Assuming constant temperature, eqs. (3)-(5) yield

$$\mathbf{J} = -D(\varepsilon_p) \text{ ¡Error!} \qquad (6)$$

Adopting material (Lagrangian) description of the medium, the obvious consideration of mass balance [*21*] with the flux defined by expression (6) leads to the equation of stress-strain assisted diffusion (cf. [*12,17*])

$$\text{¡Error!} = D\left[\nabla^2 C - \mathbf{M} \bullet \nabla C - NC\right] + \nabla D \bullet \left[\nabla C - \mathbf{M}C\right] \qquad (7)$$

where coefficients are

$$\mathbf{M} = \nabla \ln K_S \qquad (8)$$

$$N = \nabla^2 \ln K_S \qquad (9)$$

For most applications where the hydrogen environment effect on crack growth is of interest, hydrogen entry conditions may be characterised by the equilibrium value of concentration on metal surface C_Γ [*12,17*]. Then, accounting for (5), the boundary condition is

$$C_\Gamma = C_0\, K_{S\varepsilon}(\varepsilon_p(\Gamma)) \exp(\Omega\, \sigma(\Gamma)) \qquad (10)$$

where C_0 is the equilibrium hydrogen concentration provided by the environment in the bare metal (free of stress and plastic strain).

For solids under conditions of uniform environmental hydrogen activity characterised by an equilibrium concentration value $C_0 = const$, it is easy to get the exact *steady-state solution* of eq. (7) of stress-strain assisted diffusion which is asymptotically attained at $t \to \infty$. This corresponds to the equilibrium state when the diffusion flux (6) is zero or, equivalently, when the diffusion driving force (3) is null. This is provided when $C/K_S = const$. Then the steady-state solution is

$$C_\infty(K,x,y) = C_0\, K_{S\varepsilon}\big(\varepsilon_p(K,x,y)\big) \exp(\Omega\, \sigma(K,x,y)) \qquad (11)$$

With $\varepsilon_p = 0$, $K_{S\varepsilon} = 1$ and the last expression coincides with that for stress-only driven concentration [*4*].

4.2. Numerical approach: finite element formulation of the hydrogen diffusion problem

With regard to near-tip hydrogen diffusion, accounting for large deformations of the body is essential since they notably change diffusion distances in the zone of interest. The standard weighted residual process [*22*] to build up the finite element approximation to the initial-boundary value problem (7)-(10) is performed in material (Lagrangian) coordinates.

The results of the large-deformation elastoplastic stress-strain field simulations considered in the previous paragraphs (cf. Fig. 3) were taken as the input data. Diffusion modelling was performed in one-dimensional (1D) approximation along the x-axis or crack line, as described elsewhere [*23*]. The calculations were performed for an ambient temperature $T = 293$ K. The following data were considered in the computations [*4,11,14*]: $V_H = 2 \cdot 10^{-6}$ m^3/mol and $D = 10^{-12}$ m^2/s. The applied loading rate in modelling the rising load SSR tests was taken to be $dK/dt = 0.25$ MPa·m$^{1/2}$/s.

The results of the diffusion calculations (Fig. 4), are valid for whichever particular value of D provided the loading rate is adjusted to maintain the constant ratio $D/(dK/dt)$, considering the similitude criteria for the transport eq. (7), so that availability of the exact value of D for the steel under consideration is not a crucial matter. Analysis of diffusion was performed during the rising load phase from $K = 0$ after pre-cracking to $K = K_{IC}$, i.e., during the diffusion time $t_R = K_{IC}/(dK/dt)$.

The generated numerical results on crack tip hydrogen diffusion presented in Fig. 4 and complementary stress evolution data in Fig. 3 show that in the very close vicinity of the entry surfaces $x \lesssim 2 \ldots 4$ μm the concentration patterns $C(x,t)$ for fixed diffusion times t (or applied load levels $K = dK/dt \cdot t$) are quite similar to the respective stress profiles $\sigma(x)$, so that the steady-state equilibrium concentration is approximately achieved at this depths under the tried loading rate. In

deeper material points, a delay of hydrogenation due to heavier fatigue pre-cracking is observed.

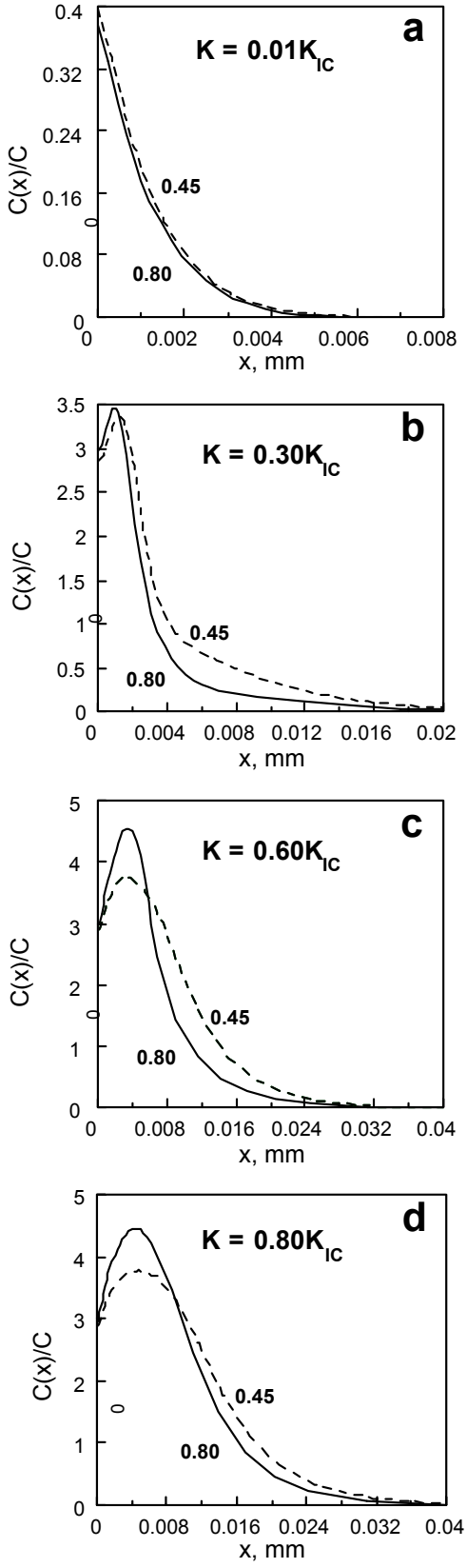

Fig. 4. Hydrogen concentration distributions ahead of the crack tip during constant-rate monotonic loading at SSR test after fatigue pre-cracking at K_{max}/K_{IC} = 0.45 (dashed lines) and 0.80 (solid lines) at progressive applied K levels. The distance x from the crack tip is measured in the deformed configuration.

5. DISCUSSION

5.1. Mechanical aspects

To analyze the results of the SSR tests on the basis of the performed simulation of the crack tip mechanics, it is useful to obtain the critical value of the stress intensity factor for HAC to proceed, K_{QHAC}, from the ratio of the failure load in hydrogen F_{HAC} to the failure load in air F_C (Fig. 1) as follows

$$K_{QHAC} = \text{¡Error!}K_{IC}(\text{air}) \qquad (12)$$

K_{QHAC} may be considered as an upper bound estimate for the threshold stress intensity factor K_{IHAC}. Neglecting subcritical crack growth the two values are the same, and in this case the fracture initiation coincides with the final fracture instant.

The stress-dependent component of the flux (6) provides acceleration of hydrogen diffusion towards the sites of maximum hydrostatic stress and delays it if negative stress gradient $\nabla\sigma < 0$ is met along the penetration path. Considering the evolutions of stress-patterns ahead of the blunting crack tip during rising load SSR tests after various pre-cracking histories (Fig. 3), it follows that heavier pre-cracking produces higher residual compressive stress and more negative stress gradient persisting over greater depth ahead of the crack tip during longer portion of the rising-load path or loading time under constant-rate loading, which are both represented by the K/K_{IC} ratio. This way, higher K_{max} during pre-cracking delays crack tip hydrogenation in the rising load SSR tests and improves resistance against hydrogen assisted fracture. This is consistent with the fundamental experimental fact displayed in Fig. 1 of HAC behaviour improvement by heavier pre-cracking regimes.

From Fig. 3 it follows that the paths of the hydrostatic stress extremum near the crack tip $\sigma^+ = \max\{\sigma(x), x > 0\}$ corresponding to monotonic load route after different pre-cracking regimes K_{max} should proceed too close to each other, so that the maximum value of σ cannot be a cause of the notable effect of pre-cracking on HAC through its influence on diffusion. On the other hand, at the initial stages of the SSR tests (applied $K \cong 0.40K_{IC}$) when the local minima of stress $\sigma^- = \min\{\sigma(x), x > 0\}$ still exists in the process zone, the value of $\sigma^-(K)$ goes substantially lower for the pre-cracking at $K_{max2} = 0.80K_{IC}$ than after fatigue at $K_{max1} = 0.45K_{IC}$ (cf. Fig. 3). This K_{max}-controlled compression, which produces underdevelopment of tensile hydrostatic stresses, persists over the zone of interest during a considerable portion of a SSR test, which provides a reason for the delay of the near-tip hydrogen accumulation by stress assisted diffusion as a consequence of a more severe pre-cracking program.

As a summary of the discussion on mechanical aspects reflected in the hydrostatic stress profiles plotted in Fig.

3, it is possible to say that, during the monotonic loading at the SSR tests in the range $0 \le K \le K_{QHAC}$, the near-tip stress field due to the milder fatigue regime $K_{max} = 0.45K_{IC}$ provides higher hydrogenation of the deeper material cells, whereas the very-near surface region is under the effect of the more elevated stresses arising when the crack is subjected to the heavier pre-cracking procedure with $K_{max} = 0.80K_{IC}$.

5.2. Chemical aspects

The equations of *stress-and-strain* assisted diffusion of hydrogen (6)-(7) may be simplified by neglecting the spatial variability of the solubility K_S and of the diffusivity D which are in general dependent on the equivalent plastic strain ε_p, i.e., taking K_S and D as some constant averaged values of $K_S(\varepsilon_p)$ and $D(\varepsilon_p)$ over the zone of interest. It is acceptable as the first approximation, since dislocations and other trap density which affect hydrogen solubility and mobility attain a certain *saturation level* with rising plastic strain [*24*]. Thus the terms with ∇K_S and ∇D are omitted and eqs. (6) and (7) yield those for *stress-only* assisted diffusion

$$\mathbf{J} = - D \nabla C + DC\Omega \nabla \sigma \qquad (13)$$

$$\textbf{¡Error!} = D \left[\nabla 2C - \mathbf{M} \bullet \nabla C - NC \right] \qquad (14)$$

The boundary condition condition for diffusion (10) and the equilibrium concentration of hydrogen (11) have an exponential dependence on hydrostatic stress σ. In the 1D case analyzed here they take respectively the form

$$C_\Gamma = A \ \exp(\Omega\sigma(\Gamma)) \qquad (15)$$

$$C_\infty(x) = A \ \exp(\Omega\sigma(x)) \qquad (16)$$

According to the results of the near-tip stress-strain field analysis displayed in Fig. 3, the evolution of $\sigma(\Gamma)$ during monotonic loading after fatigue pre-cracking is fairly insensitive to K_{max} and the same applies for the boundary condition (15). On the other hand, eq. (16) indicates that the shapes of the hydrostatic stress laws $\sigma(x)$ in the near-tip domain $x > 0$ are important for the crack tip hydrogenation. During load rise in the SSR test up to intermediate levels of applied $K \approx 0.30K_{IC}$

Fig. 3 shows substantial differences in the close vicinity of the crack tip between the two distributions of the hydrostatic stress associated with fatigue pre-cracking levels of $K_{max}/K_{IC} = 0.45$ and 0.80. These distinctions imply different rates of hydrogen transport to prospective fracture nuclei by stress assisted diffusion flux (17) driven along the x-axis by the hydrostatic stress gradient $\partial\sigma/\partial x$.

In particular, it is seen in Figs. 3a and 3b that, until $K/K_{IC} \approx 0.30$, notably more negative values of both the stress $\sigma < 0$ and its gradient $\partial\sigma/\partial x < 0$ persist ahead of the crack tip for the heavier fatigue program $K_{max} = 0.80K_{IC}$ than those for $K_{max} = 0.45K_{IC}$. This enhances hydrogen diffusion towards the fracture nuclei in the interior according to eq. (18) and explains the different hydrogen concentration profiles obtained in Figs. 4a and 4b for $K_{max}/K_{IC} = 0.45$ and 0.80.

5.3. Micromechanics of HAC

From the micromechanical point of view, in Fig. 3d it is seen that the depth of maximum hydrostatic stress is about 8 μm at the fracture instant $K_{QHAC} = 0.8K_{IC}$ corresponding to the pre-cracking at $K_{max}/K_{IC} = 0.80$, approximately the same as the respective TTS depth (Fig. 2). Therefore, the *theoretical* distance over which the stress field favours hydrogen diffusion is close to the *real physical* size of the hydrogen-assisted micro-damaged region. If one considers the stress distribution corresponding to the hydrogen assisted fracture event after pre-cracking at $K_{max}/K_{IC} = 0.45$, i.e., for $K_{QHAC} = 0.6K_{IC}$ shown in Fig. 3c, the position of maximum hydrostatic stress at fracture is fairly the same: 8μm in this case too, i.e., $x_\sigma^+(K_{QHAC}) \approx 8$ μm for both K_{max}. It is confirmed by the stress distributions at load levels when HAC occurs after different pre-cracking regimes: at $K_{QHAC1} = 0.60K_{IC}$ for $K_{max1}/K_{IC} = 0.45$ in Fig. 3c; at $K_{QHAC2} = 0.80K_{IC}$ for $K_{max2}/K_{IC} = 0.80$ in Fig. 3d. This indicates that this dimension represents some microstructural scale of the local fracture process: the size of a material unit cell or grain that must be hydrogenated to advance HAC. In addition, since the axial σ_{yy} and the hydrostatic σ stresses have their maxima approximately at the same material point, this yields the same location of possible fracture initiation site x_c assuming that a critical stress criterion of local fracture is operative, $x_c = x_\sigma^+(K_{QHAC}) = 8$ μm, which again suggests that the distance x_c may be a relevant micro-scale of local rupture in HAC. On the basis of these facts, the role of the fatigue pre-cracking on HAC initiation, which is attributed to the the post-cycling residual stresses near the crack tip, may be examined through concentration evolution data just at the afore-said critical location x_c. Although it may be observed in the plots of Fig. 4, the patterns of concentration $C(x_c,t)$ in Fig. 5 provide a better resolution of the effect. They confirm a notable delay of hydrogenation of the responsible material unit at x_c just in the domain of interest $K_{QHAC} < K_{IC}$ due to residual stresses produced by the heavier fatigue precracking.

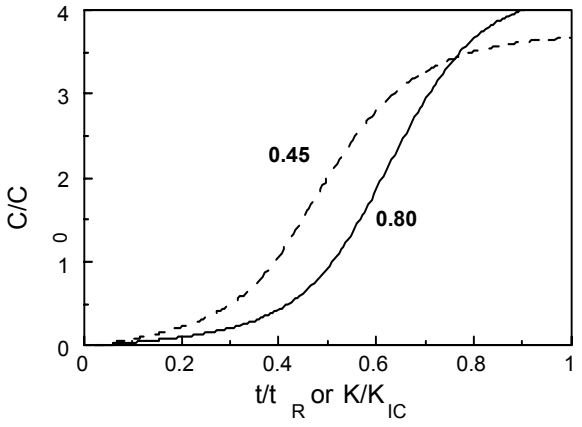

Fig. 5. Evolutions of the hydrogen concentration at the prospective fracture loci near the crack tip $x_c = 8$ μm during the constant-rate rising load SSR tests after pre-

cracking regimes at K_{max}/K_{IC} = 0.45 (dashed line) and 0.80 (solid line); the diffusion time is $t_R = K_{IC}/(dK/dt)$.

6. CONCLUSIONS

Cyclic accumulation of plastic strain and creation of the domain of compressive residual stresses improve the HAC behaviour through the increase of the failure load in aggressive environment by delaying the entry of hydrogen into the fracture process zone near the crack tip due to the existence of negative gradients of hydrostatic stress in the vicinity of the crack tip in the most severe fatigue pre-cracking program.

From the mechanical point of view, the numerical results of a high-resolution elastic-plastic finite element analysis show that hydrostatic stress distributions depend markedly on the fatigue pre-cracking level K_{max}, and this dependence is stronger at the first stages of the monotonic load phase associated with the SSR test during which the heaviest fatigue program induces compressive residual stresses in the near-tip area.

The depth of the maximum hydrostatic stress point at the fracture instant coincides with the size of the region affected by the hydrogen at the microscopical level. Therefore, the theoretical distance over which the stress field favours hydrogen diffusion is close to the real physical dimension of the hydrogen-assisted micro-damaged region detectable by scanning electron microscopy in the form of a special topography (TTS).

Since the axial and the hydrostatic stresses have their maxima approximately at the same material point, the depth of the maximum tensile (or hydrostatic) stress should be a relevant microstructure scale to mark the prospective fracture loci. This idea is consistent with the previous conclusion based on micromechanics of HAC after fractographic analysis of the broken samples.

From the chemical point of view, the results of stress assisted hydrogen diffusion computations show that hydrogen accumulation in the vicinity of the crack tip also depends on previous cyclic loading, the effects being clearly detectable in the prospective fracture loci associated with the maximum tensile (and hydrostatic) stress or, accordingly, with the region of hydrogen-assisted micro-damage.

Acknowledgments

The financial support (Grant MAT2002-01831) of this work by the Spanish Ministry of Science and Technology (MCYT) and FEDER is gratefully acknowledged. In addition, the authors wish to express their gratitude to EMESA TREFILERIA S.A. (La Coruña, Spain) for providing the steel used in the experimental programme.

REFERENCES

[*1*] Judy, R. W., Jr., King, W. E., Jr., Hauser II, J. A., and Crooker, T. W., "Influence of Experimental Variables on the Measurement of Stress Corrosion Cracking Properties of High-Strength Steels," *Environmentally Assisted Cracking: Science and Engineering, ASTM STP 1049*, W.B. Lisagor, T.W. Crooker and B.N. Leis, Eds., American Society for Testing and Materials, Philadelphia, 1990, pp. 410-422.

[*2*] Toribio, J. and Lancha, A. M., "Overload Retardation Effects on Stress Corrosion Behaviour of Prestressing Steel," *Construction and Building Materials*, Vol. 10, 1996, pp. 501-505.

[*3*] Toribio, J., Lancha, A. M., and Elices, M. "Characteristics of the New Tearing Topography Surface," *Scripta Metallurgica et Materialia*, Vol. 25, 1991, pp. 2239-2244.

[*4*] Van Leeuwen, H. P., "The Kinetics of Hydrogen Embrittlement: A Quantitative Diffusion Model," *Engineering Fracture Mechanics*, Vol. 6, 1974, pp. 141-161.

[*5*] Suresh, S., *Fatigue of Materials*, Cambridge University Press, Cambridge, 1991.

[*6*] McMeeking, R. M., "Finite Deformation Analysis of Crack-Tip Opening in Elastic-Plastic Materials and Implications for Fracture," *Journal of the Mechanics and Physics of Solids*, Vol. 25, 1977, pp. 357-381.

[*7*] Toribio, J. and Kharin, V., "High-Resolution Numerical Modelling of Stress-Strain Fields in the Vicinity of a Crack Tip Subjected to Fatigue," *Fracture From Defects (ECF12)*, M.W. Brown, E.R. de los Ríos and K.J. Miller, Eds., EMAS, West Midlands, 1998, pp. 1059-1064.

[*8*] Kanninen, M. F. and Popelar, C. H., *Advanced Fracture Mechanics*, Oxford University Press, New York , 1985.

[*9*] Handerhan, K. J. and Garrison, W. M., Jr., "A Study of Crack Tip Blunting and the Influence of Blunting Behavior on the Fracture Toughness of Ultra High Strength Steels," *Acta Metallurgica et Materialia*, Vol. 40, 1992, pp. 1337-1355.

[*10*] *MARC User Information*, Marc Analysis Research Corporation, Palo Alto, 1994.

[*11*] Hirth, J. P., "Effects of Hydrogen on the Properties of Iron and Steel," *Metallurgical Transactions*, Vol. 11A, 1980, pp. 861-890.

[*12*] Toribio, J. and Kharin, V., "Evaluation of Hydrogen Assisted Cracking: The Meaning and Significance of the Fracture Mechanics Approach," *Nuclear Engineering and Design*, Vol. 182, 1998, pp. 149-163.

[*13*] Panasyuk, V. V., Andreikiv, A. Ye. and Kharin, V. S., "Model of Crack Growth in Deformed Metals under the Action of Hydrogen," *Soviet Materials Science*, Vol. 23, 1987, pp. 111-124.

[*14*] Gerberich, W. W., Chen, Y. T., and John, C. St., "A Short-time Diffusion Correlation for Hydrogen-induced Crack Growth Kinetics," *Metallurgical Transactions*, Vol. 6A, 1975, pp. 1485-1498.

[*15*] Panasyuk, V. and Kharin, V., "The Influence of Hydrogenating Environments on Crack Propagation in Metals," *Environment Assisted Fatigue*, P. Scott and R.A. Cottis, Eds., Mechanical Engineering Publications, London, 1990, pp. 123-144.

[*16*] Kharin, V. S. "Crack Growth in Deformed Metals under the Action of Hydrogen," *Soviet Materials Science*, Vol. 23, 1987, pp. 348-357.

[*17*] Toribio, J. and Kharin, V., "*K*-dominance Condition in Hydrogen Assisted Cracking: The Role of the Far Field," *Fatigue and Fracture of Engineering Materials and Structures*, Vol. 20, 1997, pp. 729-745.

[*18*] Itatani, M., Miyoshi, Y., and Ogura, K. C., "A Numerical Analysis of Hydrogen Concentration at the Crack Tip in Austenitic Stainless Steel," *Journal of the Society of Materials Science Japan*, Vol . 40, 1991, pp. 1079-1085.

[*19*] Perng, T. P. and Altstetter, C. J., "Effects of Deformation on Hydrogen Permeation in Austenitic Stainless Steels," *Acta Metallurgica*, Vol. 34, 1986, pp. 1771-1781.

[*20*] Kronshtal, O. and Kharin, V., "Influence of Material Inhomogeneity and Variation of Temperature on Hydrogen Diffusion as a Risk Factor of Enhancement of Metals Hydrogen Degradation," *Soviet Materials Science*, Vol. 28, 1992, pp. 475-486.

[*21*] Malvern, L.E., *Introduction to the Mechanics of a Continuous Medium*, Prentice Hall, Englewood Cliffs, 1969.

[*22*] Zienkiewicz, O.C. and Morgan, K., *Finite Elements and Approximation*, John Wiley and Sons, New York, 1983.

[*23*] Toribio, J. and Kharin, V., "Role of Fatigue Crack Closure Stresses in Hydrogen Assisted Cracking. *Advances in Fatigue Crack Closure Measurement and Analysis: Second Volume*, *ASTM STP 1343*, R.C. McClung and J.C. Newman, Jr., Eds., American Society for Testing and Materials, West Conshohocken, PA, 1999, pp. 440-458.

[*24*] Kummick, A. J. and Johnson, H. H., "Deep Trapping States for Hydrogen in Deformed Iron," *Acta Metallurgica*, Vol. 28, 1980, pp. 33-39.